Check for updates

ADVANCED THEORY AND SIMULATIONS
www.advtheorysimul.com

Investigation of Tungsten-Based Seleno-Chevrel Compounds with Different Compositions for Efficient Water Splitting

Tugce Sevinc Dag, Gokhan Surucu, Aysenur Gencer, Ozge Surucu, Faruk Ozel, and Yasemin Ciftci*

This study investigates the photocatalytic water splitting performance for $Ni_xW_6Se_8$ ($x = 1, 2, 3, 4$) Chevrel phases with the chemical formula $M_xMo_6Ch_8$, where M is a metal and Ch is a chalcogen, with *x* being 0, 1, 2, 3, or 4. Density Functional Theory (DFT) is used to study the $Ni_xW_6Se_8$ ($x = 1, 2, 3, 4$) Chevrel phases, which includes earth-abundant elements for this specific study as an essential consideration for photocatalytic water splitting. The electronic properties are calculated for the NiW_6Se_8 and $Ni_2W_6Se_8$ compounds with thermodynamical, mechanical, and dynamic stabilities. For photocatalytic water splitting, the band gaps below 1.23 eV are excluded, and the conduction and valence band levels are determined to examine the reduction and oxidation potentials for efficient photocatalytic water-splitting materials. An examination of the selected band gaps, along with the conduction and valence band levels, reveals that NiW_6Se_8 is suitable for both reduction and oxidation reactions; whereas, $Ni_2W_6Se_8$ is a convenient material only for the reduction reaction. This is the first attempt, as far as the literature reveals, to study Chevrel phases in detail and to identify a suitable compound for photocatalytic water splitting.

1. Introduction

The world of today is increasingly exposed to severe weather patterns—among them, heat waves, storms, floods, droughts, and landslides—due to the effect of global warming on the climate.[1] Global warming is a result of an increase in greenhouse gases, such as carbon dioxide, methane, nitrous oxide, etc.[2] The main reason for the rise in these gas levels is the consumption of fossil fuels[3] which has doubled since 1980.[4] Therefore, researchers are on the outlook for clean, sustainable, and renewable energy sources to replace fossil fuels in the future. Hydrogen energy is one of these energy sources that is clean, abundant, and has high-energy density.[5] However, certain issues need to be addressed before the hydrogen alternative can be available worldwide. For an economy on this bases, the first step is the hydrogen production, which is necessary to guarantee sustainability.[6] Hydrogen production is possible using nuclear power, natural gas, coal gasification and, in particular, renewable energy sources.[7] Among the clean alternatives, photocatalytic water splitting is the option that uses the sunlight to generate hydrogen.

In 1972, Fujishima and Honda[8] demonstrated that the TiO_2 electrode generates photocatalytic hydrogen. However, the TiO_2 electrode has a large band gap and absorbs only UV light, limiting its applications in photocatalysis.[9] Since the pioneering work of Fujishima and Honda,[8] several semiconductors have been investigated for photocatalytic water splitting which absorb not only UV light,

T. S. Dag, Y. Ciftci
Department of Physics
Gazi University
Ankara 06500, Türkiye

G. Surucu
Department of Energy Systems Engineering
Gazi University
Ankara 06500, Türkiye
E-mail: gokhansurucu@gazi.edu.tr

A. Gencer
Department of Physics
Karamanoglu Mehmetbey University
Karaman 70200, Türkiye

O. Surucu
Department of Electrical and Electronics Engineering
Atilim University
Ankara 06836, Türkiye

F. Ozel
Department of Metallurgical and Materials Engineering
Karamanoglu Mehmetbey University
Karaman 70200, Türkiye

The ORCID identification number(s) for the author(s) of this article can be found under https://doi.org/10.1002/adts.202300336

© 2023 The Authors. Advanced Theory and Simulations published by Wiley-VCH GmbH. This is an open access article under the terms of the Creative Commons Attribution License, which permits use, distribution and reproduction in any medium, provided the original work is properly cited.

DOI: 10.1002/adts.202300336

25130390, 2023, 11, Downloaded from https://onlinelibrary.wiley.com/doi/10.1002/adts.202300336 by Atilim University, Wiley Online Library on [10/12/2023]. See the Terms and Conditions (https://onlinelibrary.wiley.com/terms-and-conditions) on Wiley Online Library for rules of use; OA articles are governed by the applicable Creative Commons License

but also visible light. For this process, the required steps include light absorption, separation, and transfer of the photogenerated carriers, and redox (reduction and oxidation) reactions at the surface.[10] Research is ongoing to identify a photocatalyst that has visible light absorption, high economic efficiency, high stability, a suitable band gap, and convenient redox potential levels.[11] For this purpose, several materials, including ternary oxides, metal chalcogenides, carbon-based materials, etc.,[12,13] have been considered as alternatives; nevertheless, none possess all the necessary requirements for an efficient photocatalyst. Among these materials, $CuInS_2$ is considered for the photocatalytic water splitting with its superior properties as suitable band gap, environment friendly elements, etc.[14] However, $CuInS_2$ has some drawbacks like photo-corrosion, high cost of In element, etc.[14] Cu_2ZnSnS_4 is an another emerging material for the photocatalytic water splitting with non-toxic and earth-abundant elements, low band gap, etc.[15] Despite these properties, Cu_2ZnSnS_4 has some issues to be considered as phase composition, crystallinity, relatively narrow band gap, etc.[15] In addition, to get an efficient photocatalyst, the heterostructures with $CuInS_2$ and Cu_2ZnSnS_4 are considered.[14,15] Despite these efforts, the research on an efficient photocatalyst is ongoing. To fill this gap and contribute to the literature, this study is designed to examine the $Ni_xW_6Se_8$ ($x = 1, 2, 3, 4$) Chevrel phase compounds in terms of their photocatalytic water-splitting performance. The Chevrel phases were initially discovered by Chevrel and Sergent in 1971[16] to have superior physical and chemical properties[17] with a chemical formula as $M_xMo_6Ch_8$, where M is a metal, Ch is a chalcogen, and x is 0, 1, 2, 3, or 4.[17] The six Mo atoms form an octahedron, while the eight chalcogen atoms construct a distorted pyramid that engulfs the octahedron.[18] The M atoms could be monovalent, divalent, trivalent, or rare-earth elements resulting in several candidates for Chevrel phases. In the literature, these is an interest for the Chevrel phases for the photocatalytic water splitting[19–22] and in this study, the $Ni_xW_6Se_8$ ($x = 1$, 2, 3,4) Chevrel phase compounds are considered where the W atoms are to be replaced instead of the Mo atoms due to being in the same group on the periodic table. Also, the Chevrel phases with the Mo atoms are commonly considered in the literature and there is a lack of interest for the Chevrel phases with the W atoms. This study could fill this gap and could be a guide to the future experimental studies. In addition, the compounds subject to this study are all earth-abundant elements; this is a crucial factor for large-scale applications in the future. The study presents the photocatalytic water-splitting performance of $Ni_xW_6Se_8$ ($x = 1$, 2, 3,4) Chevrel phase compounds using density functional theory, making it the first attempt of this kind as far as the authors are concerned with respect to the literature. It is hoped that this research can serve as a stepping stone for future attempts to shed light on these compounds.

2. Computational Details

In this study, the Vienna Ab-initio Simulation Package (VASP)[23,24] is used for the density functional theory (DFT)[25,26] calculations to investigate the structural, mechanical, dynamical, and electronic properties of the $Ni_xW_6Se_8$ ($x = 1, 2, 3, 4$) Chevrel phase compounds. The Perdew, Burke, and Ernzerhof (PBE) functional in the Generalized Gradient Approximation (GGA)[27,28] is used to define the exchange and correlation energy for the electron–electron interactions. The electron–ion interactions are also defined using the Projected Augmented Wave (PAW) method.[29] In addition to the GGA-PBE method, the Heyd–Scuseria–Ernzerhof (HSE) method[30] is employed to investigate electronic band structures. To be applied in HSE, we obtain the screened HSE06 hybrid functional using the screening parameter of 0.2 Å. Next, we add to the exchange part 25% of the precise non-local Hartree–Fock exchange.[31] The cut-off energy is chosen 700 eV, and the k-points are generated using a gamma-centered scheme[32] with ($10 \times 10 \times 10$) ($8 \times 7 \times 7$), ($7 \times 7 \times 7$), and ($7 \times 9 \times 6$) k-points for NiW_6Se_8, $Ni_2W_6Se_8$, $Ni_3W_6Se_8$, and $Ni_4W_6Se_8$, respectively. The valence electron configurations are used as $3d^84s^2$, $5d^46s^2$, and $4s^24p^4$ for Ni, W, and Se atoms, respectively. The energy and force convergence tolerances are set as 1×10^{-11} eV per atom and 1×10^{-6} eV Å^{-1}, respectively. The mechanical properties are calculated with the stress-strain method implemented in VASP.[33,34] The three-dimensional directional dependence for Young's modulus, linear compressibility, shear modulus, and Poisson's ratio for $Ni_xW_6Se_8$ compounds are obtained with the ELATE software package.[35] The dynamical properties are calculated with the linear response method using the PHONOPY software package.[36]

3. Structural Properties and Stability Considerations

The Chevrel phase compounds with the $M_xMo_6Ch_8$ chemical formula mostly crystallize in a rhombohedral hexagonal symmetry (space group $R\bar{3}$).[37] Two different structures are mentioned in the Chevrel phases, as per the literature, depending on the M element. In the first type, the M element has small cations and, in the second type, it has large cations. Especially in compounds with small cations, as the value of x in the general chemical formula changes, there are phase transitions (from $R\bar{3}$ to $P\bar{1}$).[38,39] While NiW_6Se_8 crystallizes in rhombohedral symmetry, as a result of these phase transitions, $Ni_2W_6Se_8$, $Ni_3W_6Se_8$, and $Ni_4W_6Se_8$ have a triclinic structure (space group $P\bar{1}$). The crystal structures of the $Ni_xW_6Se_8$ Chevrel phase compounds are shown in **Figure 1**, and the optimized lattice constants, lattice angles, and formation energies for the $Ni_xW_6Se_8$ compounds are presented in **Table 1**. It is necessary to calculate the formation energy to be able to investigate the structural stability of a compound. The formation energies of the optimized compounds are calculated using Equation (1).

$$\Delta E_f = E^{Ni_xW_6Se_8} - \left(xE^{Ni} + 6E^{W} + 8E^{Se}\right) \quad (1)$$

In Equation (1), $E^{Ni_xW_6Se_8}$ is the total energy, and E^{Ni}, E^{W}, and E^{Se} are the energies of one Ni, one W, and one Se atom, respectively. A negative value for formation energy indicates that the material is thermodynamically stable and can be synthesized experimentally. According to the calculated values listed in Table 1, NiW_6Se_8 and $Ni_2W_6Se_8$ are thermodynamically stable with negative formation energies, while $Ni_3W_6Se_8$ and $Ni_4W_6Se_8$ are thermodynamically unstable because of positive formation energies.

After determining thermodynamic stability, the elastic constants of the $Ni_xW_6Se_8$ compounds are investigated using the

© 2023 The Authors. Advanced Theory and Simulations published by Wiley-VCH GmbH

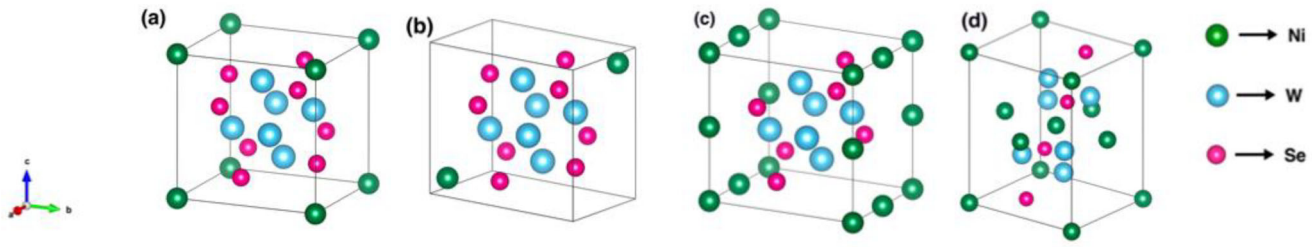


Figure 1. The crystal structures of a) NiW_6Se_8, b) $Ni_2W_6Se_8$, c) $Ni_3W_6Se_8$, and d) $Ni_4W_6Se_8$ compounds.

Table 1. The calculated lattice constants (a, b, and c in Å), lattice angles (α, β, γ), and formation energies (ΔE_f, in eV per atom) of NiW_6Se_8 ($x = 1$, 2, 3, 4) compounds.

Compound	a	b	c	α	β	γ	ΔE_f
NiW_6Se_8	6.71	6.71	6.71	93.31	93.31	93.31	−0.21
$Ni_2W_6Se_8$	6.64	6.83	6.83	97.62	89.74	95.88	−0.19
$Ni_3W_6Se_8$	6.63	6.90	6.77	95.28	94.21	94.61	0.00
$Ni_4W_6Se_8$	7.04	6.18	8.44	102.12	97.25	104.26	0.11

Table 2. The calculated elastic constants (C_{ij} in GPa) for $Ni_xW_6Se_8$ ($x = 1$, 2, 3, 4) compounds.

Compound	C_{11}	C_{12}	C_{13}	C_{14}	C_{15}	C_{33}	C_{44}
NiW_6Se_8	136.88	39.11	41.62	18.87	20.12	141.77	25.63
$Ni_2W_6Se_8$	137.94	72.88	45.84	12.09	6.58	173.66	44.44
$Ni_3W_6Se_8$	115.62	47.28	35.12	19.03	3.44	121.75	27.07
$Ni_4W_6Se_8$	90.61	76.39	39.91	−6.38	−2.09	121.38	31.14

stress–strain method implemented in the VASP.[34] This is essential as it provides information about mechanical stability. The calculated elastic constants are presented in **Table 2**. The number of independent elastic constants varies depending on crystal symmetry; in a rhombohedral system, seven elastic constants are required, while this number is twenty-one in a triclinic system. Table 2 presents only the elastic constants common to the rhombohedral system for the four $Ni_xW_6Se_8$ compounds.

In order to be mechanically stable, the elastic constants of a material must meet the Born stability criteria,[40] which are provided in Equation (2) for a rhombohedral system and in Equation (3) for a triclinic system.[41]

$$\begin{aligned} &C_{11} > |C_{12}|,\ C_{44} > 0 \\ &(C_{13})^2 < \tfrac{1}{2} C_{33}(C_{11} + C_{12}) \end{aligned} \tag{2}$$

$$\begin{aligned} &(C_{14})^2 + (C_{15})^2 < \tfrac{1}{2} C_{44}(C_{11} - C_{12}) \\ &C_{11} - C_{12} > 0 \\ &C_{11} + 2C_{12} > 0 \\ &C_{44} > 0 \end{aligned} \tag{3}$$

According to the calculated elastic constants in Table 2, the $Ni_xW_6Se_8$ ($x = 1, 2, 3, 4$) compounds are mechanically stable due to satisfying the Born stability criteria given in the equations. These constants are applied to obtain certain mechanical properties, such as bulk modulus (B), shear modulus (G), Young's modulus (E), Poisson's ratio, G/B, and B/G ratios. The mechanical properties of the $Ni_xW_6Se_8$ ($x = 1, 2, 3, 4$) compounds are listed in Table S1 (Supporting Information). Bulk modulus (or incompressibility) measures the compression of a mass under pressure that surrounds it, and it describes the response of a material to hydrostatic pressure. Shear modulus is the ratio of shear stress to the shear strain. Young's modulus, otherwise known as the modulus of elasticity, is the ratio of stress to strain. Based on the calculated values in Table S1 (Supporting Information), $Ni_2W_6Se_8$ has the highest bulk modulus (B), shear modulus (G), and Young's modulus (E), indicating that this compound has the highest stiffness among these materials. The Poisson's ratio is the ratio of transverse strain to axial strain, providing information about the bonding properties of a material. A value of 0.25 indicates dominantly ionic bonding, and 0.1 means dominantly covalent bonding.[42] The G/B ratio can also be used to interpret the bonding character; a value of 0.6 for this ratio corresponds to dominantly ionic bonding, while 1.1 corresponds to dominantly covalent bonding. According to the calculated Poisson's ratios and the G/B ratios, the $Ni_xW_6Se_8$ compounds have dominantly ionic bonding. The B/G ratio, also called the Pugh's ratio,[43] provides information about brittleness and ductility; materials with a B/G ratio above 1.75 are ductile, while those below 1.75 are brittle.[44] In addition to the B/G ratio, a positive value for Cauchy pressure, which can be obtained with C_{12}–C_{44}, indicates ductility, and a negative value indicates brittleness. According to Table S1 (Supporting Information), the $Ni_xW_6Se_8$ compounds are ductile materials.

Apart from the calculated mechanical properties, the three-dimensional directional dependences of Young's modulus, linear compressibility, Poisson's ratio, and shear modulus for these compounds are plotted with the ELATE software, as shown in Figure S1 (Supporting Information). Spherical shapes indicate isotropy, while non-spherical shapes indicate anisotropy. The degree of anisotropy is proportional to the deviation from sphericity. According to Figure S1 (Supporting Information), the linear compressibility is isotropic only for NiW_6Se_8, and the other parameters are anisotropic for all four compounds. Moreover, the blue and green shapes, respectively, correspond to the maximum and minimum values listed in Table S2 (Supporting Information). The negative values are also displayed in red, as shown in Figure S1 (Supporting Information). As can be seen, only the Poisson's ratio has negative values for these materials. Similar to auxetic materials, the negative value of the Poisson's ratio denotes perpendicular expansion occurring when stretching is applied.

© 2023 The Authors. Advanced Theory and Simulations published by Wiley-VCH GmbH

25130390, 2023, 11, Downloaded from https://onlinelibrary.wiley.com/doi/10.1002/adts.202300336 by Atilim University, Wiley Online Library on [10/12/2023]. See the Terms and Conditions (https://onlinelibrary.wiley.com/terms-and-conditions) on Wiley Online Library for rules of use; OA articles are governed by the applicable Creative Commons License

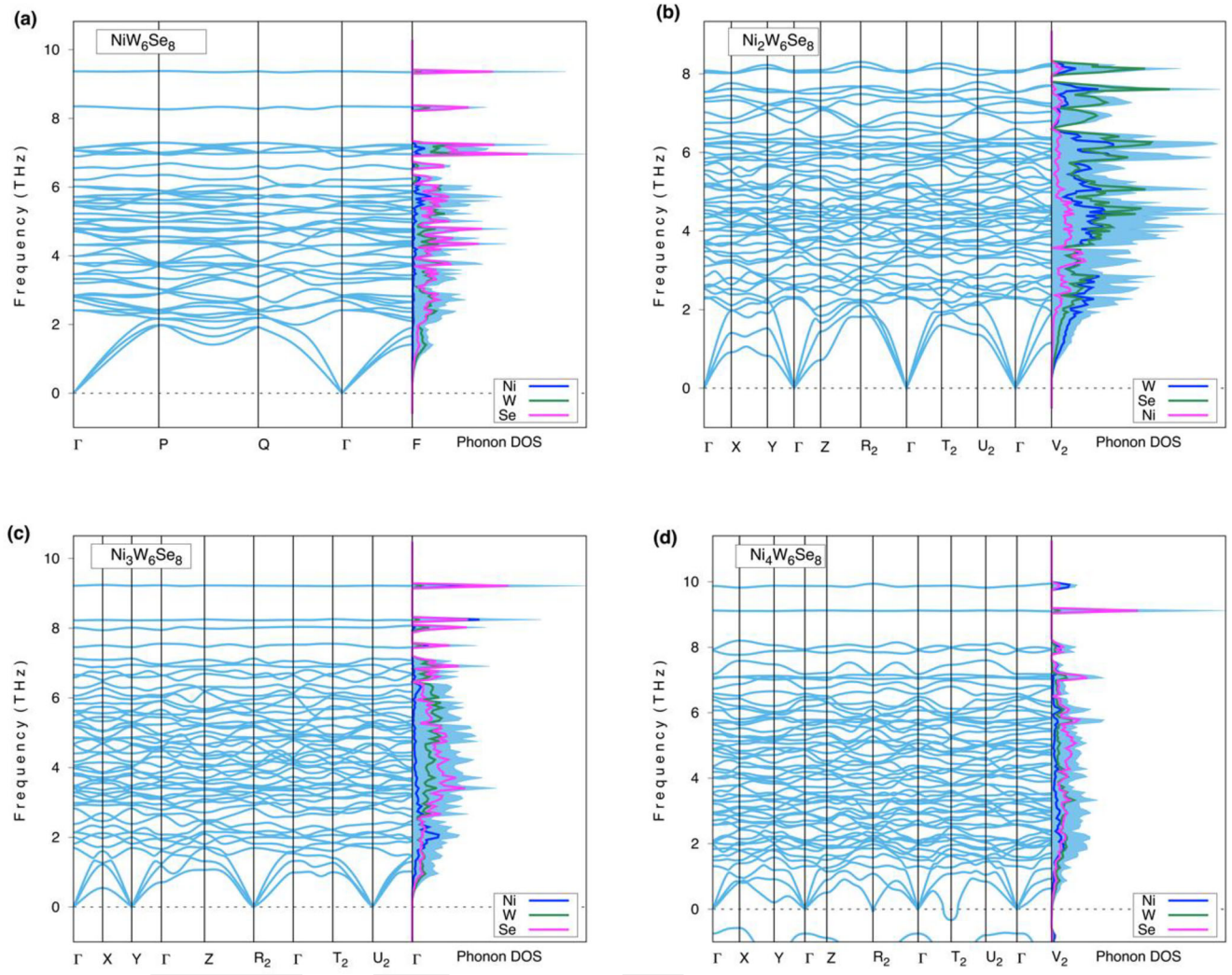


Figure 2. Phonon dispersion curves with the phonon density of states for a) NiW_6Se_8, b) $Ni_2W_6Se_8$, c) $Ni_3W_6Se_8$, and d) $Ni_4W_6Se_8$ compounds.

In this section, another criterion, dynamical stability, is examined. Therefore, the phonon dispersion curves of the $Ni_xW_6Se_8$ compounds with the phonon density of states (DOS) are plotted in **Figure 2**. Here, it should be noted that no soft mode must appear for negative frequency in order to ensure dynamical stability. Therefore, based on Figure 2, the NiW_6Se_8, $Ni_2W_6Se_8$, and $Ni_3W_6Se_8$ compounds are dynamically stable. On the other hand, the negative frequency in the $Ni_4W_6Se_8$ compound makes it dynamically unstable. The NiW_6Se_8 compound has 15 atoms in the unit cell, implying 3 acoustic and 42 optic phonon branches. The $Ni_2W_6Se_8$ has 16 atoms in the unit cell and 3 acoustic and 45 optic branches are seen in the Figure 2. $Ni_3W_6Se_8$ has 17 atoms in the unit cell, and there are 3 acoustic and 48 optic branches. Moreover, as can be seen from the phonon DOS curves, the Se atoms contribute more to higher frequencies.

After examining the thermodynamical, mechanical, and dynamical stability of the compounds, in the next section the electronic properties are studied for the $Ni_xW_6Se_8$ ($x = 1, 2$) compounds which have met the above-mentioned stability conditions.

4. Electronic Properties and Water Splitting Performances

The electronic properties of the $Ni_xW_6Se_8$ ($x = 1, 2$) compounds are studied to examine their photocatalytic water-splitting performances. To do so, the electronic band structures and the partial density of states (DOS) of the NiW_6Se_8 and $Ni_2W_6Se_8$compounds are obtained using a GGA-PBE functional in **Figures 3** and **4**, respectively. In these figures, the dotted lines indicate the Fermi levels. As seen in Figures 3a and 4a, the valence band maximums and the conduction band minimums are located at different points; thus, making these band gaps indirect as 1.03 and 0.73 eV for NiW_6Se_8 and $Ni_2W_6Se_8$, respectively. Besides, according to the partial density of states, as respectively shown in Figures 3b and 4b for NiW_6Se_8 and $Ni_2W_6Se_8$, it is seen that the most contribution comes from the d orbitals of the Ni and W atoms for both compounds, and the most contribution for the Se atoms comes from the p orbitals. For a photocatalyst to split water and produce hydrogen, it must have a suitable band gap (minimum 1.23 eV) and also, in order to use

© 2023 The Authors. Advanced Theory and Simulations published by Wiley-VCH GmbH

25130390, 2023, 11, Downloaded from https://onlinelibrary.wiley.com/doi/10.1002/adts.202300336 by Atilim University, Wiley Online Library on [10/12/2023]. See the Terms and Conditions (https://onlinelibrary.wiley.com/terms-and-conditions) on Wiley Online Library for rules of use; OA articles are governed by the applicable Creative Commons License

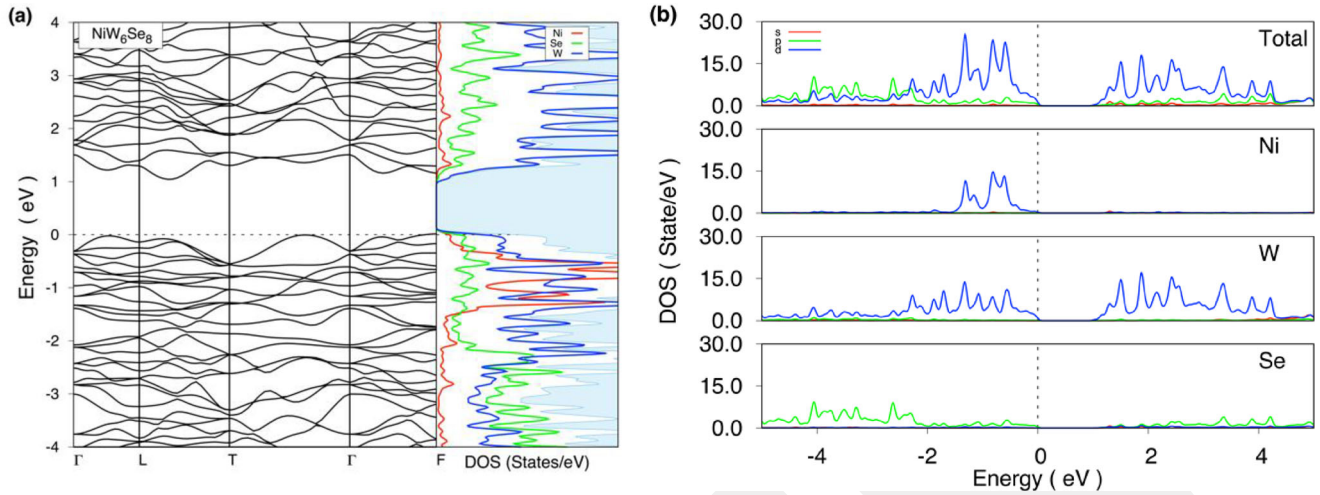


Figure 3. The electronic band structures with the density of states (DOS) and the total and partial density of states (PDOS) for the NiW_6Se_8 compound.

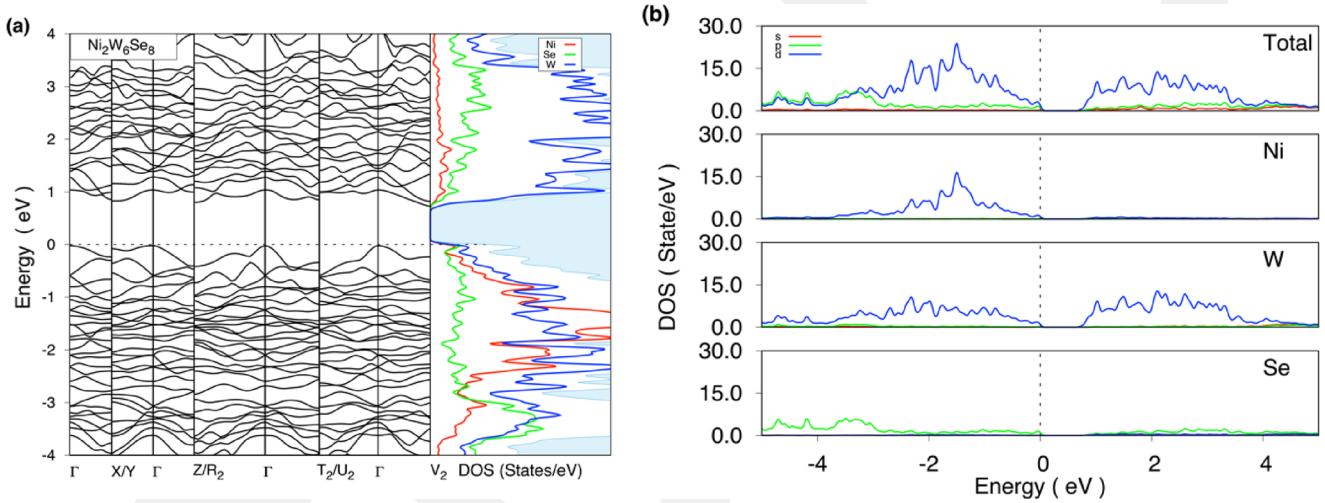


Figure 4. The electronic band structures with the density of states (DOS) and the total and partial density of states (PDOS) for the $Ni_2W_6Se_8$ compound.

visible light, the band gap is expected to be <3 eV.[45] What is more, a photocatalyst must have an appropriately located conduction band and a valence band to carry out redox (reduction and oxidation) reactions.[46] Materials with a band gap of less than 1.23 eV are not useful for photocatalytic water splitting. As seen from Figures 3a and 4a, the band gaps obtained for the $Ni_xW_6Se_8$ ($x = 1, 2$) compounds are less than 1.23 eV; however, these band gaps are obtained with a GGA-PBE functional. It is known in the literature that conventional GGA-PBE calculations underestimate the band gap.[47] To amend this, hybrid functionals can be used. To this end, the electronic band structures of the $Ni_xW_6Se_8$ ($x = 1, 2$) compounds are studied using the Heyd–Scuseria–Ernzerhof (HSE) functional[30] to obtain the band gaps consistent with the experimental results. The calculated electronic band structures are shown in **Figure 5**a,b for the NiW_6Se_8 and $Ni_2W_6Se_8$compounds, respectively. In these figures, the band structures obtained using the GGA-PBE and HSE functionals are given together to compare the results easily. Black lines indicate the band structures obtained using GGA-PBE, and red lines indicate the structures obtained using HSE. As seen in the figures, the band gaps increase to 1.39 and 1.23 eV for NiW_6Se_8 and $Ni_2W_6Se_8$, respectively. These band gaps are suitable for photocatalytic water splitting. Therefore, the next stage will be to determine the conduction and valence band levels to decide whether these compounds are suitable for the redox reactions.

To initiate redox reactions, the valence band maximum (VBM) must be more positive than the water oxidation level (O_2/H_2O, 1.23 eV vs Normal Hydrogen Electrode (NHE)); whereas, the conduction band minimum (CBM) must be more negative than the hydrogen evolution potential (H^+/H_2, 0 eV vs NHE).[48] If the CBM is more negative than the hydrogen reduction potential, the electrons in the conduction band starts the reduction process to produce hydrogen gas. If the VBM is more positive than the oxidation potential of the water, the holes in the valence band oxidize the water to form oxygen gas. For the compounds with suitable

© 2023 The Authors. Advanced Theory and Simulations published by Wiley-VCH GmbH

25130390, 2023, 11, Downloaded from https://onlinelibrary.wiley.com/doi/10.1002/adts.202300336 by Atilim University, Wiley Online Library on [10/12/2023]. See the Terms and Conditions (https://onlinelibrary.wiley.com/terms-and-conditions) on Wiley Online Library for rules of use; OA articles are governed by the applicable Creative Commons License

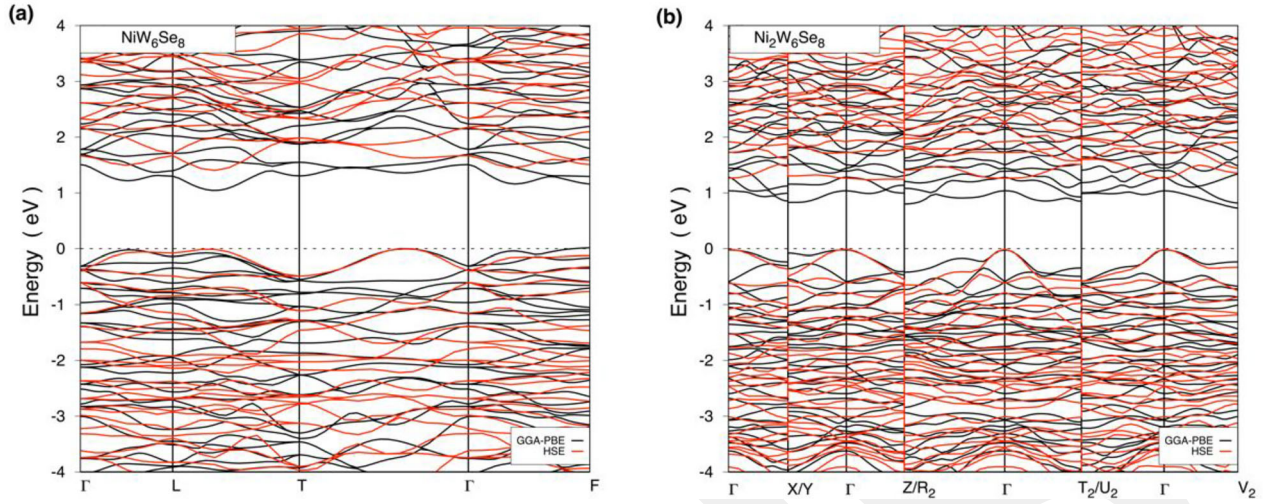


Figure 5. The electronic band structures for a) NiW_6Se_8 and b) $Ni_2W_6Se_8$ compounds. Black lines indicate structures obtained with GGA-PBE and red lines, those with HSE06.

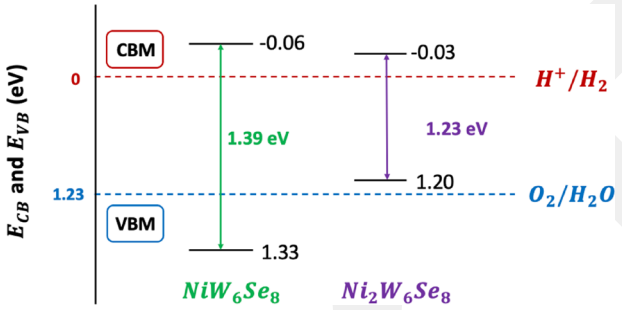


Figure 6. The schematic representation of the calculated band levels for NiW_6Se_8 and $Ni_2W_6Se_8$.

band gaps for photocatalytic water splitting, the band levels are calculated using Equations (4) and (5).[49]

$$E_{\mathrm{CBM}} = \chi - E_{\mathrm{e}} - \frac{1}{2}E_{\mathrm{g}} \tag{4}$$

$$E_{\mathrm{VBM}} = E_{\mathrm{CB}} + E_{\mathrm{g}} \tag{5}$$

In Equations (4) and (5), E_{CBM} and E_{VBM} are the positions of the conduction band minimum and valence band maximum, respectively, χ is the absolute electronegativity of the semiconductor, E_{e} is the energy of free electrons on the hydrogen scale (4.5 eV), and E_{g} is the band gap of the semiconductor. The schematic representation of the calculated band levels is shown in **Figure 6**, including the required VBM and CBM levels for photocatalytic water splitting. It can be observed that the conduction band minimums are more negative than the required CBM level for both compounds. The calculated CBM levels for NiW_6Se_8 and $Ni_2W_6Se_8$ are −0.06 and −0.03 eV, respectively, which means they have sufficient potential to reduce hydrogen. The valence band maximums are calculated as 1.33 and 1.20 eV for NiW_6Se_8 and $Ni_2W_6Se_8$, respectively. Although the VBM of NiW_6Se_8 is suitable for producing oxygen by oxidizing water due to having a higher positive VBM level than the required 1.23 eV, the VBM of $Ni_2W_6Se_8$ is not so as it has a lower positive VBM level than this value. It can, therefore, be concluded that the NiW_6Se_8 is convenient for producing both hydrogen and oxygen at the same time, and that $Ni_2W_6Se_8$ can only be used to produce hydrogen.

5. Conclusion

In this study, the $Ni_xW_6Se_8$ ($x = 1, 2, 3, 4$) compounds are investigated within the framework of DFT by examining their structural, mechanical, and dynamical stability and electronic band structures using the VASP software. The formation energies are calculated, and the structural stability of the compounds is determined. Accordingly, the $Ni_xW_6Se_8$ ($x = 1, 2$) compounds are found to be thermodynamically stable and experimentally synthesizable. Then, the mechanical and dynamical stabilities are examined. Once again, the $Ni_xW_6Se_8$ ($x = 1, 2$) compounds are observed to have both mechanical and dynamical stability. Next, the electronic band structures of the compounds are studied in detail to investigate their water-splitting performances. The band gaps calculated with GGA-PBE are 1.03 and 0.73 eV, which are lower than the 1.23 eV required for a photocatalyst to split water. These band gaps are calculated using the HSE functional, based on which the band gaps are 1.39 eV for NiW_6Se_8 and 1.23 eV for $Ni_2W_6Se_8$. The band levels are also calculated to determine whether or not there exists any photocatalytic activity. Investigations show that NiW_6Se_8 is suitable to split water and simultaneously produce hydrogen and oxygen. On the other hand, $Ni_2W_6Se_8$ can only reduce hydrogen due to the negative conduction band, but its valence band potential does not have sufficient oxidation ability. According to these results, NiW_6Se_8 has the ability to redox reactions for photocatalytic water splitting to generate hydrogen and oxygen.

This paper illustrates that the NiW_6Se_8 compound, which is composed of earth-abundant elements and has the advantage of photocatalytic performance, is a potential candidate for hydrogen and oxygen production for large-scale industrial applications. As far as the literature review has revealed, there has been no theoretical or experimental study of this material so far. The present

© 2023 The Authors. Advanced Theory and Simulations published by Wiley-VCH GmbH

25130390, 2023, 11, Downloaded from https://onlinelibrary.wiley.com/doi/10.1002/adts.202300336 by Atilim University, Wiley Online Library on [10/12/2023]. See the Terms and Conditions (https://onlinelibrary.wiley.com/terms-and-conditions) on Wiley Online Library for rules of use; OA articles are governed by the applicable Creative Commons License

work is also the first theoretical investigation, and it is hoped to be beneficial and encourage experimental studies in the future.

Supporting Information

Supporting Information is available from the Wiley Online Library or from the author.

Acknowledgements

The numerical calculations reported in this paper were performed at TUBITAK ULAKBIM, High Performance and Grid Computing Center (TRUBA resources). This work was supported by TUBITAK under project number 120F305.

Conflict of Interest

The authors declare no conflict of interest.

Author Contributions

T.S.D.: Data curation, Visualization, Writing–original draft. G.S.: Conceptualization, Methodology, Validation, Writing–review and editing. A.G.: Investigation, Visualization, Writing–original draft. O.S.: Investigation, Writing–review and editing. F.O.: Conceptualization, Writing–review and editing. Y.C.: Investigation, Software, Writing–review and editing.

Data Availability Statement

The data that support the findings of this study are available from the corresponding author upon reasonable request.

Keywords

Chevrel phases, density functional theory, dynamical stability, electronic properties, mechanical stability, photocatalytic water splitting

Received: May 19, 2023
Revised: June 8, 2023
Published online: June 29, 2023

[1] W. L. Filho, M. Balasubramanian, W. Purcell, S. Paz, *Environ. Sci. Eur.* **2022**, *34*, 45.
[2] N. Saklani, A. Khurana, *Int. J. Eng. Manag. Res.* **2019**, *9*, 24.
[3] S. E. Hosseini, *Fundamentals of Low Emission Flameless Combustion Its Applications*, **2022**, p. 1.
[4] Fossil Fuels – Our World in Data https://ourworldindata.org/fossil-fuels (accessed: September 30, 2022).
[5] M. R. Usman, *Renewable Sustainable Energy Rev.* **2022**, *167*, 112743.
[6] J. O. Abe, A. P. I. Popoola, E. Ajenifuja, O. M. Popoola, *Int. J. Hydrogen Energy* **2019**, *44*, 15072.
[7] H. Ishaq, I. Dincer, C. Crawford, *Int. J. Hydrogen Energy* **2022**, *47*, 26238.
[8] A. Fujishima, K. Honda, *Nature* **1972**, *238*, 37.
[9] Y. Cui, Q. Ma, X. Deng, Q. Meng, X. Cheng, M. Xie, X. Li, Q. Cheng, H. Liu, *Appl. Catal., B* **2017**, *206*, 136.
[10] H. Zhao, L. Jian, M. Gong, M. Jing, H. Li, Q. Mao, T. Lu, Y. Guo, R. Ji, W. Chi, Y. Dong, Y. Zhu, *Small Struct.* **2022**, *3*, 2100229.
[11] C. Yang, Z. Zhao, Q. Liu, *Appl. Surf. Sci.* **2022**, *577*, 151916.
[12] T. Jafari, E. Moharreri, A. S. Amin, R. Miao, W. Song, S. L. Suib, *Molecules* **2016**, *21*, 900.
[13] F. Özel, E. Arkan, H. Coskun, İ. Deveci, M. Yıldırım, M. Yıldırım, İ. Orak, M. O. Erdal, A. Sarılmaz, T. T. Ersöz, A. Koçyiğit, A. Karabulut, A. Özen, A. Aljabour, M. Kus, M. Ersöz, *Adv. Funct. Mater.* **2022**, *32*, 2207705.
[14] Y. Yang, X. Zheng, Y. Song, Y. Liu, D. Wu, J. Li, W. Liu, L. Fu, Y. Shen, X. Tian, *Int. J. Hydrogen Energy* **2023**, *48*, 3791.
[15] X. L. Zheng, Y. J. Yang, Y. H. Liu, P. L. Deng, J. Li, W. F. Liu, P. Rao, C. M. Jia, W. Huang, Y. L. Du, Y. J. Shen, X. L. Tian, *Rare Met.* **2022**, *41*, 2153.
[16] R. Chevrel, M. Sergent, J. Prigent, *J. Solid State Chem.* **1971**, *3*, 515.
[17] O. Peña, *Phys. C* **2015**, *514*, 95.
[18] S. Zhang, S. Peng, X. Dai, H. Weng, *Phys. Rev. B* **2022**, *106*, 035146.
[19] E. Genc Acar, T. Kuru, A. Sarilmaz, İ. Aksoy Çekceoğlu, G. Yanalak, E. Aslan, S. Süleyman Özel, G. Karanfil Kaçmaz, F. Özel, I. Hatay Patir, *ChemCatChem* **2023**, *15*, 202201252.
[20] T. Kuru, A. Sarilmaz, İ. A. Çekceoğlu, E. Aslan, A. Gencer, G. Surucu, F. Ozel, *J. Environ. Chem. Eng.* **2023**, *11*, 110190.
[21] J. Strachan, A. F. Masters, T. Maschmeyer, *Mater. Res. Bull.* **2021**, *139*, 111286.
[22] G. Karanfil, H. Coskun, M. Karakıs, A. Sarilmaz, A. Gencer, G. Surucu, A. Aljabour, F. Ozel, *Int. J. Hydrogen Energy* **2022**, *47*, 5326.
[23] A. Allouche, *J. Comput. Chem.* **2012**, *32*, 174.
[24] G. Kresse, J. Furthmüller, *Comput. Mater. Sci.* **1996**, *6*, 15.
[25] R. O. Jones, *Rev. Mod. Phys.* **2015**, *87*, 897.
[26] K. Capelle, *Braz. J. Phys.* **2006**, *36*, 1318.
[27] J. P. Perdew, K. Burke, M. Ernzerhof, *Phys. Rev. Lett.* **1996**, *77*, 3865.
[28] J. P. Perdew, J. A. Chevary, S. H. Vosko, K. A. Jackson, M. R. Pederson, D. J. Singh, C. Fiolhais, *Phys. Rev. B* **1993**, *48*, 4978.
[29] P. E. Blöchl, *Phys. Rev. B* **1994**, *50*, 17953.
[30] J. Heyd, G. E. Scuseria, M. Ernzerhof, *J. Chem. Phys.* **2003**, *118*, 8207.
[31] A. V. Krukau, O. A. Vydrov, A. F. Izmaylov, G. E. Scuseria, *J. Chem. Phys.* **2006**, *125*, 224106.
[32] J. D. Pack, H. J. Monkhorst, *Phys. Rev. B* **1977**, *16*, 1748.
[33] Y. Le Page, P. Saxe, *Phys. Rev. B: Condens. Matter Mater. Phys.* **2002**, *65*, 104104.
[34] V. Wang, N. Xu, J. C. Liu, G. Tang, W. T. Geng, *Comput. Phys. Commun.* **2021**, *267*, 108033.
[35] R. Gaillac, P. Pullumbi, F.-X. Coudert, *J. Phys.: Condens. Matter* **2016**, *28*, 275201.
[36] A. Togo, I. Tanaka, *Scr. Mater.* **2015**, *108*, 1.
[37] Ø. Fischer, *Appl. Phys.* **1978**, *16*, 1.
[38] K. Yvon, *Solid State Commun.* **1978**, *25*, 327.
[39] E. Levi, D. Aurbach, *Chem. Mater.* **2010**, *22*, 3678.
[40] F. Mouhat, F. X. Coudert, *Phys. Rev. B: Condens. Matter Mater. Phys.* **2014**, *90*, 3.
[41] M. Born, *Math. Proc. Cambridge Philos. Soc.* **1940**, *36*, 160.
[42] A. Gencer, O. Surucu, G. Surucu, E. Deligoz, *J. Solid State Chem.* **2020**, *289*, 121469.
[43] P. Taylor, S. F. Pugh, *Philos. Mag. Ser. 7* **1954**, *45*, 823.
[44] A. Gencer, O. Surucu, D. Usanmaz, R. Khenata, A. Candan, G. Surucu, *J. Alloys Compd.* **2021**, *883*, 160869.
[45] L. Yuan, C. Han, M. Q. Yang, Y. J. Xu, *Int. Rev. Phys. Chem.* **2016**, *35*, 1.
[46] J. Sarkar, S. Bhattacharyya, *Arch. Thermodyn.* **2012**, *33*, 23.
[47] J. P. Perdew, M. Levy, *Phys. Rev. Lett.* **1983**, *51*, 1884.
[48] K. Maeda, K. Domen, *Bull. Chem. Soc. Jpn.* **2016**, *89*, 627.
[49] Y. H. Du, W. Zeng, B. Tang, F. S. Liu, Q. J. Liu, X. H. Li, M. Zhong, *J. Solid State Chem.* **2021**, *298*, 122127.

© 2023 The Authors. Advanced Theory and Simulations published by Wiley-VCH GmbH

25130390, 2023, 11, Downloaded from https://onlinelibrary.wiley.com/doi/10.1002/adts.202300336 by Atilim University, Wiley Online Library on [10/12/2023]. See the Terms and Conditions (https://onlinelibrary.wiley.com/terms-and-conditions) on Wiley Online Library for rules of use; OA articles are governed by the applicable Creative Commons License